Sewer Defect Classification using Synthetic Point Clouds

Joakim Bruslund Haurum[a,§], Moaaz M. J. Allahham[b,*], Mathias S. Lynge[c,†], Kasper Schøn Henriksen[d,‡], Ivan A. Nikolov[e,**] and Thomas B. Moeslund[f,††]
Visual Analysis of People (VAP) Laboratory, Aalborg University, Rendsburggade 14, Aalborg, Denmark
{*mallah16**, *mlynge16*†, *kshe16*‡}*@student.aau.dk*, {*joha*§, *iani***, *tbm*††}*@create.aau.dk*

Keywords: 3D Deep Learning, Defect Classification, Synthetic Data, Sewers, Point Clouds, Transfer Learning.

Abstract: Sewer pipes are currently manually inspected by trained inspectors, making the process prone to human errors, which can be potentially critical. There is therefore a great research and industry interest in automating the sewer inspection process. Previous research have been focused on working with 2D image data, similar to how inspections are currently conducted. There is, however, a clear potential for utilizing recent advances within 3D computer vision for this task. In this paper we investigate the feasibility of applying two modern deep learning methods, DGCNN and PointNet, on a new publicly available sewer point cloud dataset. As point cloud data from real sewers is scarce, we investigate using synthetic data to bootstrap the training process. We investigate four data scenarios, and find that training on synthetic data and fine-tune on real data gives the best results, increasing the metrics by 6-10 percentage points for the best model. Data and code is available at https://bitbucket.org/aauvap/sewer3dclassification.

1 INTRODUCTION

The sewerage infrastructure is one of the largest, but also most forgotten, infrastructures in our modern society. In the United States there are currently approximately 2 million km of sewer pipes serving nearly 240 million Americans. By 2036 the sewerage infrastructure is expected to serve an additional 56 million users (American Society of Civil Engineers, 2017). The size of the sewerage infrastructure poses a clear problem during maintenance, as it is near impossible to regularly inspect all stretches of sewer pipes. Furthermore, sewer maintenance requires skilled inspectors who are capable of operating the required equipment to inspect the buried pipes. These inspections are conducted using a remote-controlled "tractor", which the inspector controls from a vehicle above ground. This can be both demanding and slow, and potentially prone to human errors.

To deal with this problem, one possibility is to use an autonomous or semi-autonomous robotic solution. Such solutions have been successfully developed and deployed for tunnel walls inspection (Menendez et al., 2018), transmission and electrical wires (Qin et al., 2018), underwater ship hulls (Garrido et al., 2018), wind turbine blades (Car et al., 2020), among others. An important characteristic that each of these solutions share, is that the robotic system needs to have appropriate sensors for both self-localization and mapping the environment, as well as capturing enough information from the surfaces such that a proper inspection of potential damages or obstructions can be achieved. To ensure that enough information is captured, 3D information in the form of depth images and point clouds, is chosen in addition to traditional 2D images. To capture such information, different sensor can be used - LiDAR laser scanners (Nasrollahi et al., 2019; Ravi et al., 2020), stereo cameras (Wen et al., 2017), photogrammetry (Nielsen et al., 2020), time-of-flight and structured light cameras (Pham et al., 2016; Santur et al., 2016).

Sewer inspection data presented in the state-of-the-art is normally not available as public datasets, and the ones used are focused around 2D RGB images (Haurum and Moeslund, 2020). However, capturing large amounts of 3D inspection data from sewers is not a trivial task. Therefore, we look into using synthetic data for training a sewer inspection algorithm. The creation of such synthetic data has been detailed in the work of Henriksen et al. (2020), where

[a] https://orcid.org/0000-0002-0544-0422
[b] https://orcid.org/0000-0002-3212-0731
[c] https://orcid.org/0000-0002-8492-1274
[d] https://orcid.org/0000-0001-8660-1672
[e] https://orcid.org/0000-0002-4952-8848
[f] https://orcid.org/0000-0001-7584-5209

Haurum, J., Allahham, M., Lynge, M., Henriksen, K., Nikolov, I. and Moeslund, T.
Sewer Defect Classification using Synthetic Point Clouds.
DOI: 10.5220/0010207908910900
In *Proceedings of the 16th International Joint Conference on Computer Vision, Imaging and Computer Graphics Theory and Applications (VISIGRAPP 2021) - Volume 5: VISAPP*, pages 891-900
ISBN: 978-989-758-488-6

sewer pipes were 3D modeled and used in a custom simulation environment, together with an approximated PMD Pico Flexx (CamBoard, 2018) time-of-flight camera, to generate 3D point clouds. We therefore look into using synthetic data to bootstrap the training process of a deep learning based 3D sewer defect classifier. The main contributions of this paper are threefold:

1. A publicly available dataset of synthetic and real point clouds of normal and defective sewer pipes.
2. Demonstrating the feasibility of using 3D point clouds and geometric deep learning methods for classifying sewer defects.
3. A comparison of the effect of synthetic and/or real data when training a defect classifier.

2 RELATED WORK

Automated Sewer Inspections. Vision-based automation of sewer defects has traditionally been based on 2D image data from Closed-Circuit Television (CCTV) and Sewer Scanner and Evaluation Technology (SSET) sewer inspections. CCTV and SSET inspection data have been used for nearly 30 years, with methods ranging from morphology based discriminators (Sinha and Fieguth, 2006a,b,c; Su et al., 2011), to using feature descriptors and machine learning classifiers (Yang and Su, 2008; Wu et al., 2013; Myrans et al., 2018), and within the recent years using deep learning for classification, detection, and segmentation (Hassan et al., 2019; Li et al., 2019; Kumar et al., 2020; Wang and Cheng, 2020). For an in-depth review of these methods we refer to the survey by Haurum and Moeslund (2020). There has, however, been significantly less work on detecting defects using 3D sensors. 3D sensors are interesting as some sewer defects, such as displaced joints and obstacles, may not be immediately visually apparent, but can be obvious when looking at the depth information. Traditionally two types of sensors have been used: Laser scanners and ultrasound. Laser scanners have been used extensively by Duran *et al.* for binary defect detection of cracks, defective joints, and obstacles, by utilizing depth and the intensity of the reflected light as input for fully-connected neural networks (Duran et al., 2003, 2004, 2007). Similarly, Lepot et al. (2017) designed a novel laser scanner for detecting displaced joints, cracks, and deposits, which works in a comparable way as to CCTV inspections. Tezerjani et al. (2015) similarly proposed a novel laser scanner design for defect detection and extracting pipe geometry. Furthermore, Ahrary et al. (2006) and Kolesnik and Baratoff (2000) have used laser scanners for navigation purposes as well as detecting defects and recovering the geometry of the pipe. Iyer et al. (2012) utilized ultrasound based methods for detecting cracks and holes in concrete pipes. Khan and Patil have proposed detection cracks in PVC pipes by analyzing the acoustic response under different conditions using frequency domain analysis (Khan and Patil, 2018a,b). Alejo *et al.* have utilized RGB-D camera for localization and defect classification, utilizing graph based learning and convolutional neural networks (CNN) (Alejo et al., 2017, 2020). Furthermore, as documented by Haurum and Moeslund (2020) there is a lack of public dataset and code releases for methods based on CCTV and SSET inspections, which is also the case with methods designed for inspections using 3D sensors.

Geometric Deep Learning. Within recent years the application of deep learning methods on unstructured 3D data, such as point clouds, have gained interest within the computer vision community. The earliest methods utilized specialized voxel-based methods (Qi et al., 2016) and reutilizing 2D CNNs in a multiview-based approach (Su et al., 2015) in order to classify objects, resulting in, respectively, high memory consumption and slow computation times. Qi *et al.* were the first to successfully process the raw point clouds using the fully-connected neural network architectures, PointNet (Qi et al., 2017a) and PointNet++ (Qi et al., 2017b). This work has been expanded upon within the autonomous vehicle community for object detection and segmentation (Lang et al., 2019; Vora et al., 2020), amongst other point based methods (Zhou and Tuzel, 2018; Wang et al., 2019). 3D point clouds can also be observed as a graph problem, which was utilized by Wang et al. (2019) in the Dynamic Graph CNN (DGCNN) architecture, where edge information between points are aggregated to better learn local and global information. For a review of the geometric deep learning field we refer to the work of Bronstein et al. (2017) and Cao et al. (2020).

Synthetic Data. In the current era of machine learning based methods, representative training data is essential. However, it may not always be possible to acquire the necessary training data, as it can be prohibitively expensive. This is especially apparent when working on tasks where the interesting parts are *rare*, such as defect detection. The generation of representative synthetic data has therefore been increasingly investigated. Tobin et al. (2017) proposed the Do-

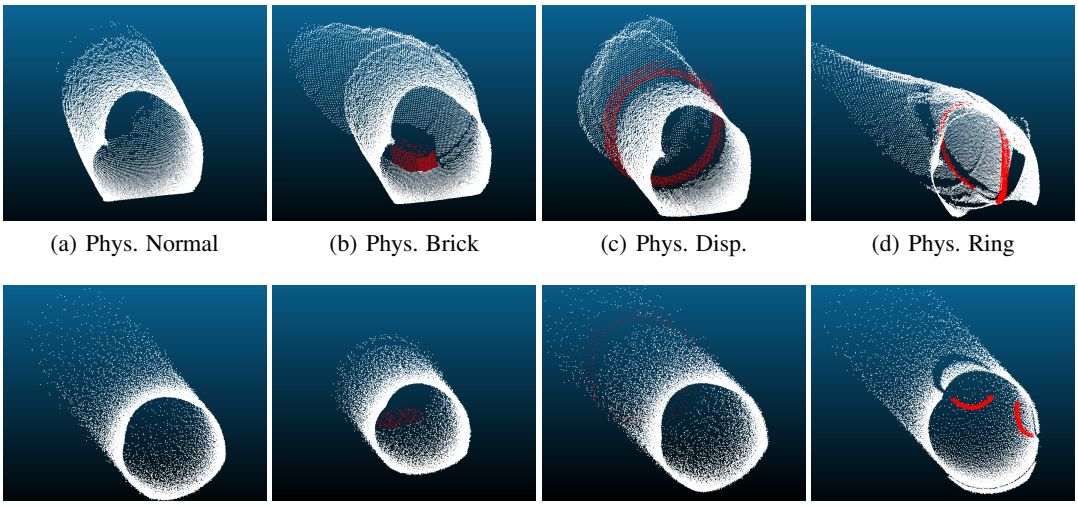

(a) Phys. Normal (b) Phys. Brick (c) Phys. Disp. (d) Phys. Ring

(e) Synth. Normal (f) Synth. Brick (g) Synth. Disp. (h) Synth. Ring

Figure 1: Example point clouds from the real and synthetic pipe setup. Defects are shown in red for easier visualization.

main Randomization (DR) method, which generates randomized renderings of a scene in order to train a robot. Prakash et al. (2019) expanded on this method by accounting for the structure in the scene, called Structured Domain Randomization (SDR), which was demonstrated on the KITTY object detection task. Beery et al. (2020) showed using large amount of synthetic data can help handle the long tailed distribution that occurs in the animal classification task, showing the promise of synthetic data. Lastly, Henriksen et al. (2020) proposed an SDR based synthetic data generator for PVC sewer pipes, which can generate displaced joints and defective rubber rings in the joints.

Figure 2: An example pipe configuration, used for collecting the point cloud data from the physical setup.

3 DATASET

As mentioned in Section 2 there are currently no publicly available datasets within the sewer inspection field. We therefore construct our own dataset, consisting of normal non-defective pipes and defective pipes with three different kinds of defects: displaced joints, defective rubber rings, and obstructions in the form of bricks. The three defect types are selected as they are observed frequently in the real world. As 3D sensors are very rarely used for sewer inspections, the constructed dataset consists of synthetic point cloud data, as well as real data obtained in a lab environment.

3.1 Synthetic Data Generation

We base our synthetic data generation on the SDR-based approach proposed by Henriksen et al. (2020). The proposed data generator generates a random sewer network consisting of clean PVC pipes, with no water or sediments, and randomly places defects along the pipes. A virtual approximation of the PMD Pico Flexx time-of-flight sensor is moved through the sewer network, and record synthetic point clouds.

The generated defects are, however, constrained to only displaced joints and defective rubber rings, which are concurrent. We update the simulator to allow displaced joints and defective rubber rings to occur independent of each other, and further extend it to allow for randomly placed bricks in the pipe. Bricks are chosen, because of their relatively basic shape, not prone to many variations, compared to other possible obstructions in sewer pipes. This way the overall defect classification performance of the algorithms can be evaluated, without the need to create too many different shape cases. The bricks are placed by applying a random force to the brick, which pushes it into a random position and orientation in the pipe. We constrain the simulator to only allow one kind of defect per extracted point cloud, in order to be able to deter-

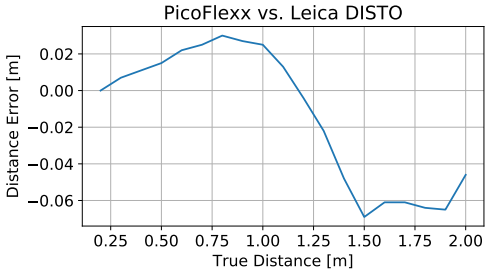

Figure 3: The Pico Flexx distance errors, compared to a laser range finder at distances between 0.2m and 2m.

mine the effect of each type of defect.

3.2 Physical Data Collection

In order to collect point clouds from a set of real PVC sewer pipes, a physical setup was created in an indoor laboratory, see Figure 2. The data was collected using a PMD Pico Flex sensor. As no sewer data captured with the Pico Flex sensor is available, we conduct a simple test, to verify its accuracy presented in its datasheet (CamBoard, 2018). The sensor is mounted on a moving platform and directed towards a white wall with an approximately Lambertian surface. The sensor is then moved away from the wall at equal 0.1m intervals, starting from 0.2m until 2m. A Leica DISTO laser range finder, is used to capture ground truth data at each position, as it has a known accuracy of 0.03m. The two sensors are calibrated to the same distance measurement at 0.2m. The difference between the two are presented on Figure 3. The distance errors are higher than the ones given in the datasheet CamBoard (2018) for the camera. This needs to be taken into account, as these distance errors, might result in noise or deformations in the selected pipe segments, especially between 0.8m and 1.5m.

Five different pipe segments, with a diameter of 400 mm were used for data collection: two straight pipes, and three corner pipes with turning angles of 15, 30, and 45 degrees. The pipe segments were combined in different permutation, with the sensor moved through the pipes while placed in the center. Defects were added to the pipes by randomly placing bricks or rubber rings in the pipes, or displacing the joints of the pipe segments. As in the synthetic data generator, only one type of defect is present at a time.

3.3 Comparison between Real and Synthetic Data

Examples of the real and synthetic data are shown in Figure 1, with one example per class. One problem found from the real data captured with the Pico Flexx sensor, is the presence of "holes" in both the depth map and the point cloud - areas, where no depth data is captured. These holes depend on the environmental lighting, the distance and orientation of the imaged surface, compared to the camera, as well as the glossiness of the surface. Examples of such holes can be seen in Figure 4. One way we address this problem is by subsampling both the synthetic and real point cloud data, which lowers the density variation of the point clouds. More information, about the subsampling process can be found in Section 4.1.

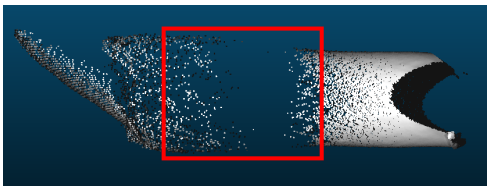

Figure 4: Example of point clouds captured with the real Pico Flexx and the holes, caused by missing data.

3.4 Dataset Split

The acquired synthetic and real data are divided into training, validation and test splits, as shown in Table 1. We choose to place the majority of the real data (85%) in the test split, as to reflect the real world data situation, where inspection data is in the form of CCTV and SSET videos and annotated 3D data is limited. Inversely, we utilize the majority of the synthetic data in the training and validation splits. We make sure there is no data leakage between splits by generating new synthetic data for each split, and splitting the real data based on the pipe segment configurations. We balance the amount of defective and normal data, such that the problem is more well-behaved, which is standard within the sewer defect classification field (Li et al., 2019; Hassan et al., 2019).

4 METHODS

The proposed method consists of two steps: preprocessing the data and the deep learning models.

4.1 Data Preprocessing

Training a deep learning model on the raw point cloud data is infeasible due to the large number of points, leading to high memory consumption. It is therefore necessary to subsample the point clouds in order to efficiently process them. Before subsampling point clouds, it is preferred to reduce the number of outliers that may occur. This can prevent subsampling

Table 1: Overview of the data in the different data splits. The Displacement (Disp.), Brick, and Rubber Ring columns represent the amount of point clouds for the three investigated defect types.

	Synthetic				Real				
Split	**Normal**	**Disp.**	**Brick**	**Rubber Ring**	**Normal**	**Disp.**	**Brick**	**Rubber Ring**	**Total**
Training	5,365	1,811	1,822	1,802	140	45	45	44	11,074
Validation	1,385	439	428	448	31	12	12	13	2,768
Test	1,350	450	450	450	244	85	76	80	3,185
Total	8,100	2,700	2,700	2,700	415	142	133	137	17,027

approaches being biased by the outliers and rather focus on points containing relevant geometric information of a given pipe. Points that are stored in the origin of a point cloud are discarded, as they represent points that did not return a valid value. Afterwards, Statistical Outlier Removal (SOR) (Barnett and Lewis, 1984) is applied to discard aberrative points that heavily differ from the geometric representation of a pipe.

We subsample the point clouds to 1024 points, the number of points originally used for the PointNet approach. Traditionally the subsampling step has been performed by applying the Farthest Point Sampling method, which iteratively selects the point in the point cloud which is farthest away from the previously selected points (Qi et al., 2017a). This is, however, not the best approach for our data, as some defects manifest themselves as points in the middle of the pipe, which would be subsequently removed. Therefore we apply two different subsampling approaches sequentially. First we apply a spatial subsampling step Rousseeuw and Leroy (2005), which enforces a minimum distance, d, between each point. d is selected such that more than 1024 points remain, though d may change per point cloud. d is initially set to 0.03, and decremented by 0.004 each time the resulting point cloud has less than 1024 points. Afterwards the point cloud is reduced to 1024 through uniformly sampling the subsampled point cloud. As a last step the subsampled point clouds are normalized into a unit sphere. Examples of a pipe segment before and after the preprocessing steps can be seen in Figure 5.

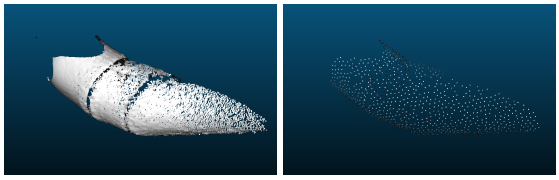

(a) Before Subsampling (b) After Subsampling

Figure 5: Example of a sewer pipe segment before and after the subsampling preprocessing steps.

4.2 Model Architectures

We investigate the performance of two state-of-the-art geometric deep learning methods: PointNet (Qi et al., 2017a) and DGCNN (Wang et al., 2019). We choose PointNet to get a baseline performance, whereas DGCNN is chosen to evaluate the effectiveness of the advances within the field. PointNet is built upon sequentially applying the same fully-connected sub-networks on the individual points, in parallel. This way each point is processed independently of any other points. In order to aggregate the feature information of each point, the symmetric max pooling function is used. Furthermore, the PointNet architecture includes a special sub-network called a T-Net, which predicts an affine transformation matrix used to align the input into a canonical form. The T-Net is applied in the beginning on the raw input, as well as the intermediate features. However, the intermediate feature alignment matrix is learned in a high dimensional space, which makes the optimization process more difficult (Qi et al., 2017a). Therefore, Qi et al. (2017a) regularize the feature alignment matrix, A, by forcing it to be close to an orthogonal matrix, as shown in Equation 1.

$$L_{reg} = ||I - AA^T||_F^2 \quad (1)$$

The DGCNN network builds upon the PointNet architecture, by introducing the EdgeConv layer between each of the shared fully-connected subnetworks. For each point, x_i, in point cloud, the EdgeConv layer finds the k closest points in the feature space, x_j, including the point itself. For all k points, a learnable edge function, denoted $h(x_i, x_j)$, is applied, and the obtained edge features are aggregated using a symmetric aggregation function. In DGCNN, h is defined as a fully-connected network which takes the concatenation of x_i and $x_j - x_i$ as input, while the aggregation function is a simple channel wise max operation. This way both global and local shape information is captured in the EdgeConv layer.

5 EXPERIMENTAL RESULTS

We approach the task as a multi-class classification task, where we have to determine whether the point

Table 2: Relevant hyperparameters and the chosen values. For the learning rate and weight decay we try all permutations of the specified values.

Parameter	Value
Learning Rate (η)	$[10^{-3}, 10^{-2}, 10^{-1}]$
Momentum	0.9
Weight Decay	$[10^{-5}, 10^{-4}, 10^{-3}, 10^{-2}, 10^{-1}]$
Dropout Rate	0.5
Batch Size	32
Epochs	50

cloud represents a sewer with one of the three considered defects, or whether it is a normal sewer pipe. The PointNet and DGCNN networks are trained and evaluated using the dataset described in Section 3. The two selected networks are trained under four different data scenarios:

S1 Train on synthetic data.

S2 Train on real data.

S3 Train on synthetic and real data.

S4 Train on synthetic data, and fine-tune on real data.

The validation and test splits consist of both real and synthetic data for all data scenarios. By testing these different data scenarios we hope to determine the effect of the synthetic data, and how to best utilize the small amount of real life data which may be available.

For each method and scenario we utilize the hyperparameters shown in Table 2 and perform grid search over the learning rate, η, and the weight decay. For DGCNN we set k to 20, while for PointNet we weight the regularization loss L_{reg} by 0.001. The models are trained for 50 epochs using Stochastic Gradient Descent (SGD) with Momentum, and cosine annealing (Loshchilov and Hutter, 2017) the learning rate from η to $\eta \cdot 10^{-2}$, and the Cross Entropy loss objective. We handle the class-imbalance between the normal pipes and three defects by weighing the loss objective differently for each class. The class weights are set as the proportion of class samples compared to the class with the most samples. Lastly, the data is augmented during training by jittering each point with noise from a Gaussian distribution, with zero mean and 0.02 standard deviation. For scenario 1, 2, and 3 we select the model which achieved the best validation loss. For scenario 4 we take the best performing model in scenario 1 and fine-tune it, with identical parameters except the selected η, which is multiplied by 10^{-1}.

We evaluate the models by considering their confusion matrices on the real test data as shown in Figure 7-8, as well as the precision, recall, and F1-score in Table 3-4. The metrics are calculated as the average of the binary metrics for each class, where each class is weighted by the proportion of the class in the dataset. We present the resulting metrics for the real test data, as well as for the full test data split. Lastly, we also investigate the effect of the ratio of real life data used when fine-tuning the models in data scenario 4. We investigate using between 0% (*i.e.* no fine-tuning) up to 100% of the real training data, in increments of 10%. The resulting metrics for the real data test split are shown in Figure 6.

Table 3: Performance of the PointNet and DGCNN networks on the real data test split, for all four data scenarios. All metrics are the weighted average across all classes.

Model	Precision	Recall	F1
PointNet-S1	3.58	15.88	5.25
DGCNN-S1	29.02	20.62	17.65
PointNet-S2	2.72	16.49	4.67
DGCNN-S2	25.31	50.31	33.68
PointNet-S3	28.61	32.16	30.23
DGCNN-S3	34.55	22.27	16.66
PointNet-S4	23.17	27.42	24.24
DGCNN-S4	39.69	26.19	23.58

Table 4: Performance of the PointNet and DGCNN networks on the entire data test split, for all four data scenarios. All metrics are the weighted average across all classes.

Model	Precision	Recall	F1
PointNet-S1	8.00	17.21	6.70
DGCNN-S1	57.57	56.73	57.09
PointNet-S2	2.77	16.64	4.75
DGCNN-S2	25.05	50.05	33.39
PointNet-S3	34.36	32.40	31.65
DGCNN-S3	58.72	57.52	58.67
PointNet-S4	28.37	36.11	30.98
DGCNN-S4	50.37	36.61	35.25

6 DISCUSSION

From the results it is evident that the DGCNN network consistently outperforms the PointNet network. Even the best performing case of PointNet, trained using data scenario 3, which scores the highest F1 score, consistently avoids predicting the rubber rings. This is a general theme throughout the trained PointNet networks, which in all other cases stick to predicting one or two classes. Comparatively, the DGCNN networks makes more well rounded predictions, with only DGCNN-S2 consistently predicting a single

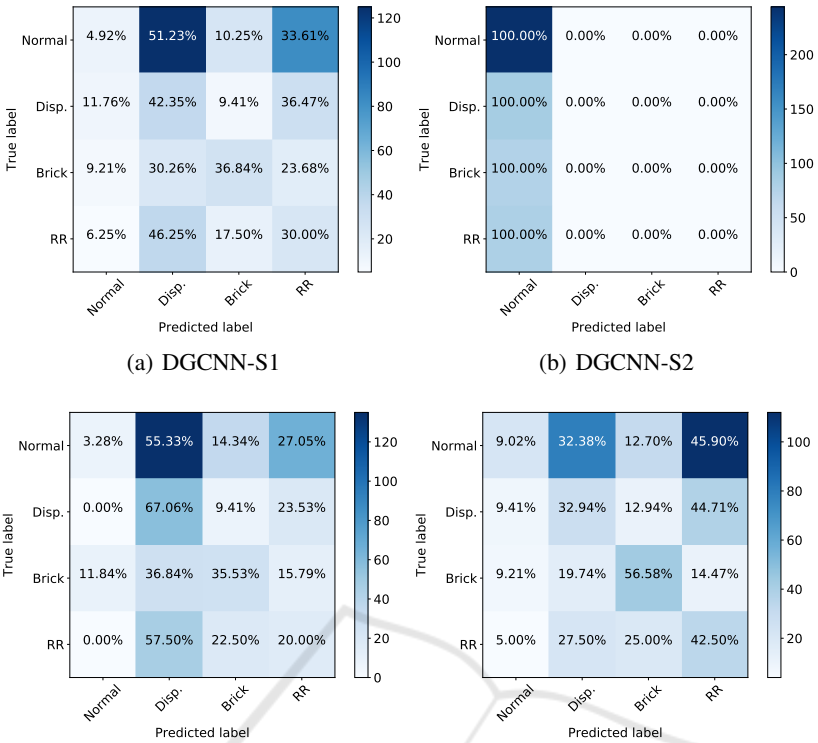

(a) DGCNN-S1 (b) DGCNN-S2

(c) DGCNN-S3 (d) DGCNN-S4

Figure 7: Confusion matrices of the real data test split, for the DGCNN architecture and four data scenarios. Disp. and RR denotes Displacement and Rubber Ring. respectively.

class. This is reflected by the consistently high metrics. Therefore, it appears that there is a clear benefit of the EdgeConv layers for the sewer defect classification task. This makes sense as both the local and the global structure is affected by defects, due to shadowing of the sensor and changes to the pipe itself.

When looking into the different data strategies, it is found that using either only synthetic or real data is a poor strategy. Instead the best results were obtained by pre-training on synthetic data, followed by fine-tuning on real data. This led to a consistent improvement over both data scenario 1 and 3 on the real data. Looking at Figure 6, we see that the ratio of real point cloud data used to fine-tune the DGCNN network is proportional to the metric performance. However, the PointNet network again converges to a point where only one or two classes are predicted, as seen in Figure 8(d). We can therefore conclude that synthetic training data can be used to bootstrap the training process of a 3D sewer defect classifier.

However, the networks are not a perfect classifier, as there are several failure points. As mentioned earlier, only one of the PointNets managed to converge to a usable classifier, with the rest instead simply predicting one or two classes. Conversely, the DGCNN converge to a more usable classifier. However, the

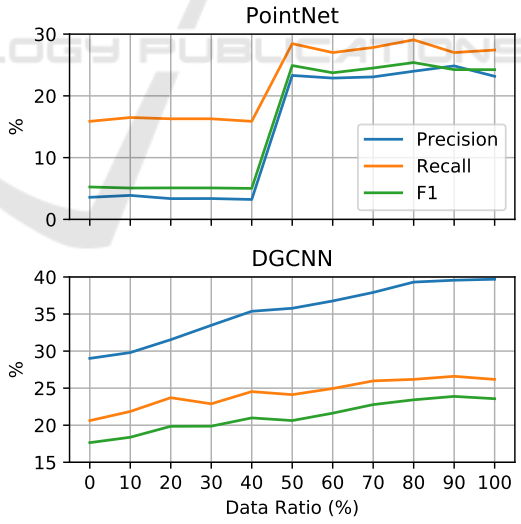

Figure 6: Plot of the evaluation metrics, when increasing the ratio of the real training data used to fine-tune the networks.

best performing model, DGCNN-S4, is biased towards the defect classes, with only 9% correctly predicted non-defective pipes in the real data. This may be due to some defects occurring quite far into the pipe, though still visible to the sensor. In these cases

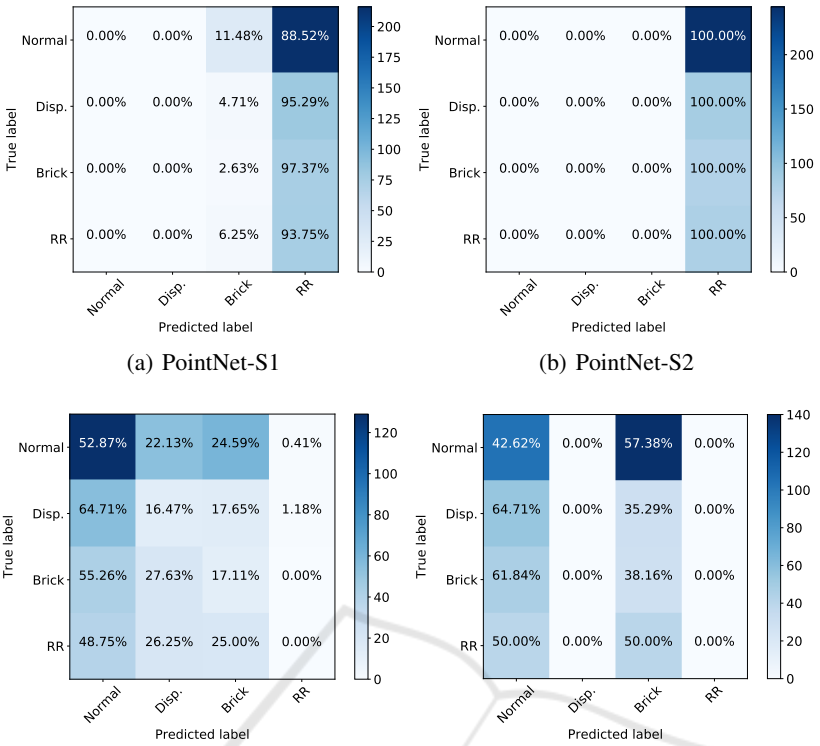

(a) PointNet-S1 (b) PointNet-S2

(c) PointNet-S3 (d) PointNet-S4

Figure 8: Confusion matrices of the real data test split, for the PointNet architecture and four data scenarios. Disp. and RR denotes Displacement and Rubber Ring. respectively.

the effect on the recorded point cloud, such as shadowing, will be quite subtle, and more easily confused with a normal sewer pipe.

7 CONCLUSION

In this work we investigate the possibility of utilizing modern geometric deep learning techniques in order to detect defects in sewer pipes, using a combination of synthetic and real point cloud data. We compare two network architectures, PointNet and DGCNN, on a new publicly available dataset with 17,000 point clouds and four classes. The dataset is structured such that the majority of the training and validation splits consist of synthetic data, with the majority of the point cloud data of real sewer pipes are reserved for the test data. We conduct a grid search for the hyperparameters, and train the chosen networks under four different training data scenarios, in order to investigate the effect of using synthetic and real training data. We find that the DGCNN networks consistently outperforms the PointNet baseline, when investigating the confusion matrices and metrics. We also find that the best performance is achieved using both synthetic and real training data, specifically when using the real data to fine-tune a network trained on synthetic data. The trained classifiers are, however, not perfect, as they tend to favor classifying defects instead of normal pipes. With these findings we show that both geometric deep learning methods and synthetic training data is viable for training sewer defect classifiers, though more work is needed for the classifiers to become more stable.

ACKNOWLEDGEMENTS

This work is supported by Innovation Fund Denmark [grant number 8055-00015A] and is part of the Automated Sewer Inspection Robot (ASIR) project. The authors declare no conflict of interests.

REFERENCES

Ahrary, A., Kawamura, Y., and Ishikawa, M. (2006). A laser scanner for landmark detection with the sewer inspection robot kantaro. In *2006 IEEE/SMC International Conference on System of Systems Engineering*.

Alejo, D., Caballero, F., and Merino, L. (2017). Rgbd-based robot localization in sewer networks. In *2017 IEEE/RSJ International Conference on Intelligent Robots and Systems (IROS)*.

Alejo, D., Mier, G., Marques, C., Caballero, F., Merino, L., and Alvito, P. (2020). *SIAR: A Ground Robot Solution for Semi-autonomous Inspection of Visitable Sewers*. Springer International Publishing, Cham.

American Society of Civil Engineers (2017). 2017 infrastructure report card - wastewater. https://www.infrastructurereportcard.org/wp-content/uploads/2017/01/Wastewater-Final.pdf. Accessed: 14-11-2020.

Barnett, V. and Lewis, T. (1984). *Outliers in Statistical Data*. Wiley Series in Probability and Statistics. Wiley.

Beery, S., Liu, Y., Morris, D., Piavis, J., Kapoor, A., Meister, M., Joshi, N., and Perona, P. (2020). Synthetic examples improve generalization for rare classes. In *2020 IEEE Winter Conference on Applications of Computer Vision (WACV)*.

Bronstein, M. M., Bruna, J., LeCun, Y., Szlam, A., and Vandergheynst, P. (2017). Geometric deep learning: Going beyond euclidean data. *IEEE Signal Processing Magazine*, 34(4).

CamBoard (2018). Development kit brief camboard pico flexx. https://pmdtec.com/picofamily/wp-content/uploads/2018/03/PMD_DevKit_Brief_CB_pico_flexx_CE_V0218-1.pdf. Accessed: 25-11-2020.

Cao, W., Yan, Z., He, Z., and He, Z. (2020). A comprehensive survey on geometric deep learning. *IEEE Access*, 8.

Car, M., Markovic, L., Ivanovic, A., Orsag, M., and Bogdan, S. (2020). Autonomous wind-turbine blade inspection using lidar-equipped unmanned aerial vehicle. *IEEE Access*, 8.

Duran, O., Althoefer, K., and Seneviratne, L. D. (2003). Pipe inspection using a laser-based transducer and automated analysis techniques. *IEEE/ASME Transactions on Mechatronics*, 8(3).

Duran, O., Althoefer, K., and Seneviratne, L. D. (2004). Automated pipe inspection using ann and laser data fusion. In *IEEE International Conference on Robotics and Automation, 2004. Proceedings. ICRA '04. 2004*, volume 5.

Duran, O., Althoefer, K., and Seneviratne, L. D. (2007). Automated pipe defect detection and categorization using camera/laser-based profiler and artificial neural network. *IEEE Transactions on Automation Science and Engineering*, 4(1).

Garrido, G. G., Sattar, T., Corsar, M., James, R., and Seghier, D. (2018). Towards safe inspection of long weld lines on ship hulls using an autonomous robot. In *21st International Conference on Climbing and Walking Robots*.

Hassan, S. I., Dang, L. M., Mehmood, I., Im, S., Choi, C., Kang, J., Park, Y.-S., and Moon, H. (2019). Underground sewer pipe condition assessment based on convolutional neural networks. *Automation in Construction*, 106.

Haurum, J. B. and Moeslund, T. B. (2020). A survey on image-based automation of cctv and sset sewer inspections. *Automation in Construction*, 111.

Henriksen, K. S., Lynge, M. S., Jeppesen, M. D. B., Allahham, M. M. J., Nikolov, I. A., Haurum, J. B., and Moeslund, T. B. (2020). Generating synthetic point clouds of sewer networks: An initial investigation. In *Augmented Reality, Virtual Reality, and Computer Graphics*, Cham. Springer International Publishing.

Iyer, S., Sinha, S. K., Pedrick, M. K., and Tittmann, B. R. (2012). Evaluation of ultrasonic inspection and imaging systems for concrete pipes. *Automation in Construction*, 22. Planning Future Cities-Selected papers from the 2010 eCAADe Conference.

Khan, M. S. and Patil, R. (2018a). Acoustic characterization of pvc sewer pipes for crack detection using frequency domain analysis. In *2018 IEEE International Smart Cities Conference (ISC2)*.

Khan, M. S. and Patil, R. (2018b). Statistical analysis of acoustic response of pvc pipes for crack detection. In *SoutheastCon 2018*.

Kolesnik, M. and Baratoff, G. (2000). Online distance recovery for a sewer inspection robot. In *Proceedings 15th International Conference on Pattern Recognition. ICPR-2000*, volume 1.

Kumar, S. S., Wang, M., Abraham, D. M., Jahanshahi, M. R., Iseley, T., and Cheng, J. C. P. (2020). Deep learning–based automated detection of sewer defects in cctv videos. *Journal of Computing in Civil Engineering*, 34(1).

Lang, A. H., Vora, S., Caesar, H., Zhou, L., Yang, J., and Beijbom, O. (2019). Pointpillars: Fast encoders for object detection from point clouds. In *2019 IEEE/CVF Conference on Computer Vision and Pattern Recognition (CVPR)*.

Lepot, M., Stanić, N., and Clemens, F. H. (2017). A technology for sewer pipe inspection (part 2): Experimental assessment of a new laser profiler for sewer defect detection and quantification. *Automation in Construction*, 73.

Li, D., Cong, A., and Guo, S. (2019). Sewer damage detection from imbalanced cctv inspection data using deep convolutional neural networks with hierarchical classification. *Automation in Construction*, 101.

Loshchilov, I. and Hutter, F. (2017). SGDR: stochastic gradient descent with warm restarts. In *5th International Conference on Learning Representations, ICLR 2017, Toulon, France, April 24-26, 2017, Conference Track Proceedings*. OpenReview.net.

Menendez, E., Victores, J. G., Montero, R., Martínez, S., and Balaguer, C. (2018). Tunnel structural inspection and assessment using an autonomous robotic system. *Automation in Construction*, 87.

Myrans, J., Everson, R., and Kapelan, Z. (2018). Automated detection of faults in sewers using cctv image sequences. *Automation in Construction*, 95.

Nasrollahi, M., Bolourian, N., and Hammad, A. (2019). Concrete surface defect detection using deep neural network based on lidar scanning. In *Proceedings of*

the CSCE Annual Conference, Laval, Greater Montreal, QC, Canada.

Nielsen, M. S., Nikolov, I., Kruse, E. K., Garnæs, J., and Madsen, C. B. (2020). High-resolution structure-from-motion for quantitative measurement of leading-edge roughness. *Energies*, 13(15).

Pham, N. H., La, H. M., Ha, Q. P., Dang, S. N., Vo, A. H., and Dinh, Q. H. (2016). Visual and 3d mapping for steel bridge inspection using a climbing robot. In *ISARC 2016-33rd International Symposium on Automation and Robotics in Construction*.

Prakash, A., Boochoon, S., Brophy, M., Acuna, D., Cameracci, E., State, G., Shapira, O., and Birchfield, S. (2019). Structured domain randomization: Bridging the reality gap by context-aware synthetic data. In *2019 International Conference on Robotics and Automation (ICRA)*.

Qi, C. R., Su, H., Mo, K., and Guibas, L. J. (2017a). Pointnet: Deep learning on point sets for 3d classification and segmentation. In *2017 IEEE Conference on Computer Vision and Pattern Recognition (CVPR)*.

Qi, C. R., Su, H., Nießner, M., Dai, A., Yan, M., and Guibas, L. J. (2016). Volumetric and multi-view cnns for object classification on 3d data. In *2016 IEEE Conference on Computer Vision and Pattern Recognition (CVPR)*.

Qi, C. R., Yi, L., Su, H., and Guibas, L. J. (2017b). Pointnet++: Deep hierarchical feature learning on point sets in a metric space. In *Advances in Neural Information Processing Systems 30*. Curran Associates, Inc.

Qin, X., Wu, G., Lei, J., Fan, F., Ye, X., and Mei, Q. (2018). A novel method of autonomous inspection for transmission line based on cable inspection robot lidar data. *Sensors*, 18(2).

Ravi, R., Bullock, D., and Habib, A. (2020). Highway and airport runway pavement inspection using mobile lidar. *The International Archives of Photogrammetry, Remote Sensing and Spatial Information Sciences*, 43.

Rousseeuw, P. J. and Leroy, A. M. (2005). *Robust regression and outlier detection*, volume 589. John wiley & sons.

Santur, Y., Karaköse, M., and Akın, E. (2016). Condition monitoring approach using 3d modelling of railway tracks with laser cameras. In *International Conference on Advanced Technology & Sciences (ICAT'16) pp*.

Sinha, S. K. and Fieguth, P. W. (2006a). Automated detection of cracks in buried concrete pipe images. *Automation in Construction*, 15(1).

Sinha, S. K. and Fieguth, P. W. (2006b). Neuro-fuzzy network for the classification of buried pipe defects. *Automation in Construction*, 15(1).

Sinha, S. K. and Fieguth, P. W. (2006c). Segmentation of buried concrete pipe images. *Automation in Construction*, 15(1).

Su, H., Maji, S., Kalogerakis, E., and Learned-Miller, E. (2015). Multi-view convolutional neural networks for 3d shape recognition. In *2015 IEEE International Conference on Computer Vision (ICCV)*.

Su, T.-C., Yang, M.-D., Wu, T.-C., and Lin, J.-Y. (2011). Morphological segmentation based on edge detection for sewer pipe defects on cctv images. *Expert Systems with Applications*, 38(10).

Tezerjani, A. D., Mehrandezh, M., and Paranjape, R. (2015). Defect detection in pipes using a mobile laser-optics technology and digital geometry. *MATEC Web of Conferences*, 32.

Tobin, J., Fong, R., Ray, A., Schneider, J., Zaremba, W., and Abbeel, P. (2017). Domain randomization for transferring deep neural networks from simulation to the real world. In *2017 IEEE/RSJ International Conference on Intelligent Robots and Systems (IROS)*.

Vora, S., Lang, A. H., Helou, B., and Beijbom, O. (2020). Pointpainting: Sequential fusion for 3d object detection. In *2020 IEEE/CVF Conference on Computer Vision and Pattern Recognition (CVPR)*.

Wang, M. and Cheng, J. C. P. (2020). A unified convolutional neural network integrated with conditional random field for pipe defect segmentation. *Computer-Aided Civil and Infrastructure Engineering*, 35(2).

Wang, Y., Chao, W., Garg, D., Hariharan, B., Campbell, M., and Weinberger, K. Q. (2019). Pseudo-lidar from visual depth estimation: Bridging the gap in 3d object detection for autonomous driving. In *2019 IEEE/CVF Conference on Computer Vision and Pattern Recognition (CVPR)*.

Wang, Y., Sun, Y., Liu, Z., Sarma, S. E., Bronstein, M. M., and Solomon, J. M. (2019). Dynamic graph cnn for learning on point clouds. *ACM Trans. Graph.*, 38(5).

Wen, X., Song, K., Niu, M., Dong, Z., and Yan, Y. (2017). A three-dimensional inspection system for high temperature steel product surface sample height using stereo vision and blue encoded patterns. *Optik*, 130.

Wu, W., Liu, Z., and He, Y. (2013). Classification of defects with ensemble methods in the automated visual inspection of sewer pipes. *Pattern Analysis and Applications*, 18(2).

Yang, M.-D. and Su, T.-C. (2008). Automated diagnosis of sewer pipe defects based on machine learning approaches. *Expert Systems with Applications*, 35(3).

Zhou, Y. and Tuzel, O. (2018). Voxelnet: End-to-end learning for point cloud based 3d object detection. In *2018 IEEE/CVF Conference on Computer Vision and Pattern Recognition*.